Diffusion-Time Distribution Analysis Reveals Characteristic Ligand-Dependent Interaction Patterns of Nuclear Receptors in Living Cells†

Hanna Jankevics, Michael Prummer, Paulina Izewska, Horst Pick, Kirsten Leufgen, and Horst Vogel*

Laboratory of Physical Chemistry of Polymers and Membranes, Institute of Chemical Sciences and Engineering, Swiss Federal Institute of Technology Lausanne (EPFL), CH-1015 Lausanne, Switzerland

Received April 22, 2005; Revised Manuscript Received June 28, 2005

ABSTRACT: Nuclear receptors initiate transcription, interact with regulatory proteins, and are influenced by hormones, drugs, and pollutants. Herein, we discover ligand-specific mobility patterns of human estrogen receptor-α (ER) in living cells using diffusion-time distribution analysis (DDA). This novel method, based on fluorescence correlation spectroscopy (FCS), is especially suited to unraveling multiple protein interactions in vivo at native expression levels. We found that ER forms a limited number of distinct complexes with a varying population by dynamic interaction with other nuclear components. Dose-response curves of different ligands could be obtained for each receptor interaction. The potential to identify interacting proteins was demonstrated by comparing DDA of the ER cofactor SRC-3 attached to yellow fluorescent protein (YFP) with those of YFP-ER. Our findings open up new routes to elucidating transcription regulation and to detecting and distinguishing pharmacologically and toxicologically active compounds in vivo. Moreover, DDA provides a general approach to monitoring biochemical networks in individual living cells.

Nuclear receptors are transcription factors that are activated via ligand binding and/or phosphorylation. Upon activation, they directly modulate gene expression by binding to specific response elements present in the promoter region of target genes. As in the case of many other receptors, nuclear receptors also function only within a complex biochemical network of numerous proteins (*1*−*3*) (Figure 1). Because nuclear receptors control many aspects of cellular metabolism, they have become the focus of intensive research in developing therapeutics in prevalent diseases such as diabetes and cancer (*4*, *5*). Nuclear receptors are also sensitively influenced by drugs or exogenous pollutants, e.g., herbicides and plasticizers. In this context, protection of humans, animals, and the ecosystem against endocrine disruptors has gained considerable attention (*6*, *7*).

Despite their wide-ranging consequences, for instance, for the development of more precisely acting medicines, quantitative details about nuclear receptor-mediated signaling are largely unknown. Such protein interaction networks are currently investigated in proteomics (*8*) and systems biology research. Presently available methods of detecting stable multiprotein complexes, like yeast two-hybrid screens (*9*), two-dimensional (2D) gel electrophoresis followed by mass spectrometry (*10*), or chromatin immunoprecipitation (*2*), show some limitations: these extracellular, in vitro proteomic assays are neither able to detect transient (weak) interactions nor are they free from the uncertainty that the detected interactions are artificially induced by high protein concentrations. Even more important, they cannot deliver a quantitative thermodynamic and kinetic description of the underlying biochemical reactions, which is the key to understanding cellular functions on a molecular basis. Therefore, optical microscopy and selective fluorescence labeling have received an increasing amount of attention because of the possibility of imaging proteins and molecular complexes in living cells with high spatial and temporal resolution, thus enabling the disentanglement of biochemical networks in vivo (*11*, *12*).

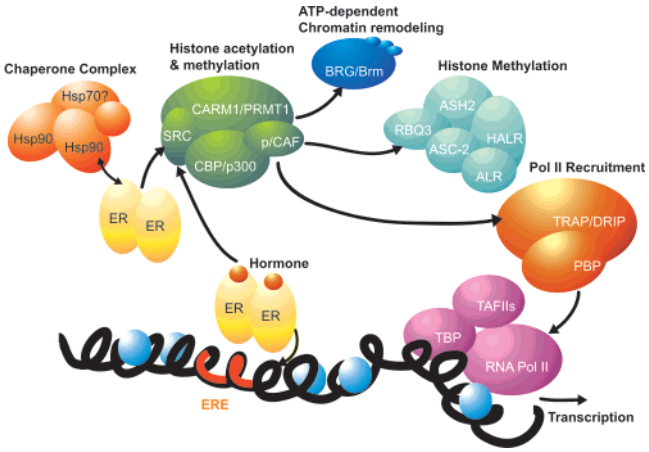

FIGURE 1: Cartoon illustrating the complexity of putative ER interactions with its partners during ligand-induced transcription activation. Prior to hormone addition, ER is present as monomer or dimer, most likely bound to a chaperone complex and possibly interacting with coregulatory proteins. Addition of hormone induces interactions of ER with an increasing number of other proteins [including chaperones (*34*), co-activators (*50*, *51*), co-repressors (*38*), histone modification complexes (*2*, *38*), and RNA polymerases (*2*)] and also increases the residence time on chromatin. This highly regulated process leads finally to transcription with the help of RNA polymerase II.

† This work was financially supported by the Swiss National Science Foundation within the national research project "Endocrine disruptors: relevance to humans, animals, and ecosystems" (NRP50), and internal funds of the EPFL.

* To whom correspondence should be addressed. Telephone: +41-21-69-33155. Fax: +41-21-69-36190. E-mail: horst.vogel@epfl.ch.

10.1021/bi050744v CCC: $30.25
Published on Web 08/11/2005

Here we investigate in living cells the complex and dynamic nature of molecular interactions of a prototypic nuclear hormone receptor, human estrogen receptor-α (ER)[1] (*13*). By analyzing distributions of diffusion times, we were able to reveal for the first time a complex mobility pattern that arises when agonists or antagonists are applied to MCF-7 breast cancer cells. The diffusion times were determined in nuclei of living cells by fluorescence correlation spectroscopy (FCS) of ER fused to yellow fluorescent protein (YFP). Our results provide evidence that the use of diffusion-time distribution analysis (DDA) as a general tool in the emerging field of "live-cell proteomics" is well conceivable (*14*). The crucial advantage of DDA compared to conventional bioanalytical tools is that it allows for the determination not only of binding partners but also of their equilibrium distributions, in living cells, at native expression levels. In the context of nuclear hormone receptors and the assessment of endocrine-disrupting compounds (EDCs), DDA can be fundamental for the development of live-cell EDC detection and toxicology assays.

EXPERIMENTAL PROCEDURES

Cell Culture and Transfection. Adherent human breast cancer cells (MCF-7) were grown in Dulbecco's modified Eagle's medium (DMEM/F-12) (Invitrogen). The medium was supplemented with 2.2% fetal calf serum (Sigma). The cultures were kept at 37 °C and 5% CO_2 and were split at regular intervals. Three days before the experiments, the medium was changed to D-MEM/F-12 without phenol red (Invitrogen) with 2.2% charcoal-treated fetal calf serum (DMEM/F-12 steroid free). Sixteen to twenty hours before transfection, exponentially growing cells were seeded either on sterile microscope cover glasses (thickness of 0.16 mm, diameter of 25 mm) placed in a six-well plate or on Lab-Tek chambered cover glass (Nalge Nunc) at a density of ~10000 cells/mL. The cells were transfected using an Effectene transfection kit (Qiagen). After 4 h at 37 °C in the incubator, the transfection medium was replaced with freshly prepared medium (DMEM/F-12 steroid free).

YFP Fusion Proteins. The expression vector for wild-type ER was a gift from B. Desvèrgne (Center for Integrative Genomics, University of Lausanne, Switzerland). The cDNA encoding ER was cloned as the PCR-amplified *Eco*RI−*Bam*I fragment (1.8 kb; forward and reverse primers being 5′-CGGAATTCCGCCATGACCATGACCTCC-3′ and 5′-CGGGATCCCGTCAGACTGTGGCAGGG-3′, respectively) into the mammalian expression vector pEYFP-C1 (Clontech), yielding the YFP−ER fusion protein (YFP−ER) (Figure 2a). The final product was verified by restriction and sequence analysis. The expression of the full-length ER fusion protein was confirmed by immunoblot analysis of nuclear extracts, prepared as described in ref *15*, with purified ER (PanVera) as a standard. For immunoblotting, a monoclonal mouse antibody directed against the ligand-binding domain (LBD) of ER was used (TE111.5D11; Neomarkers).

[1] Abbreviations: ER, human estrogen receptor-α; DDA, diffusion-time distribution analysis; FCS, fluorescence correlation spectroscopy; YFP, yellow fluorescent protein; SRC-3, steroid receptor coactivator-3; RID, receptor interaction domain of SRC-3; E2, 17β-estradiol; 4OHT, 4-hydroxytamoxifen; ICI, ICI 182,780; ACF, autocorrelation function; FRAP, fluorescence recovery after photobleaching; FRET, fluorescence resonance energy transfer; CRC, concentration response curve.

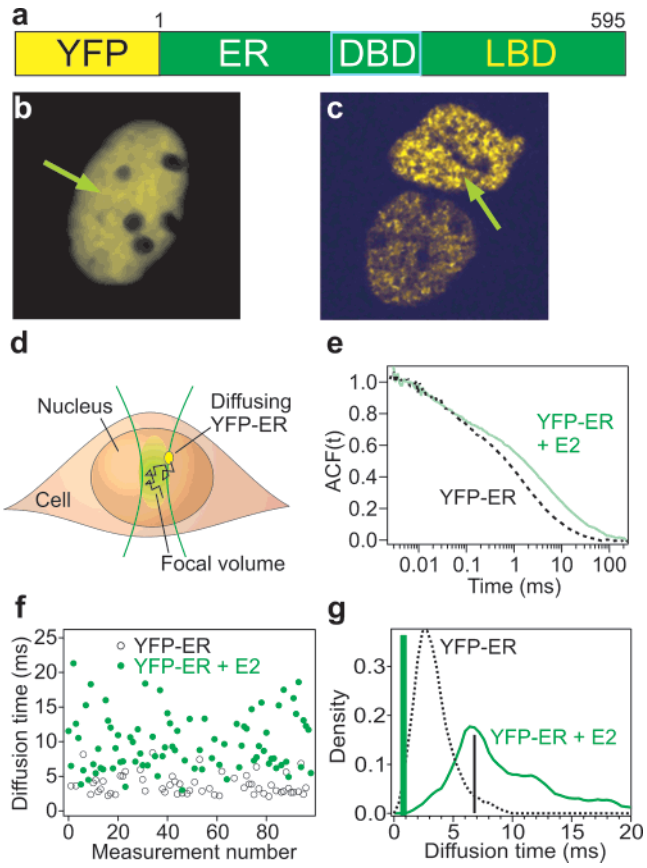

FIGURE 2: Schematic view of the experimental method and data analysis for FCS in live cells. (a) Domain structure of the YFP−ER construct. YFP was fused to the N-terminal part of ER. The major domains of ER are the DNA binding domain (DBD) and the ligand binding domain (LBD). (b) Confocal fluorescence microscopy of an MCF-7 cell expressing YFP−ER. The receptor is homogeneously distributed in the nucleus and excluded from nucleoli in the absence of ligand. (c) Two MCF-7 cells expressing YFP−ER in the nucleus after addition of a saturating concentration of E2. YFP−ER is redistributed inside the nucleus to form a speckled pattern. In panels b and c, the arrows point toward the FCS focal position inside the nuclei. (d) Schematic picture of the FCS experiment. The labeled receptor diffuses into and out of the confocal volume element inside the nucleus. The time scale of the fluctuations of the emitted intensity is characterized by the mobility of the receptor. (e) Typical experimentally obtained autocorrelation functions (ACFs) of YFP−ER for two conditions: in the absence of ligand (dashed line) and in the presence of 100 nM E2 (solid line). By applying a two-species model to these ACFs, we obtained two characteristic diffusion times. (f) Slow diffusion time τ_D from a two-species model, where the fast component was fixed to 0.8 ms, plotted vs the measurement number for 98 experiments in six cells. (g) Histogram of the data in panel f showing in addition the mean (black vertical line) and the fraction of the fast diffusive component (green vertical line).

The functional activity of YFP−ER was confirmed by two different methods: (i) a reporter gene assay using transiently transfected cells to probe the ability of YFP−ER or wtER to induce luciferase expression in a ligand-dependent manner and (ii) a radio-ligand binding assay (http://www.invitrogen.com/downloads/L0561.pdf) to determine the ligand binding affinity of YFP−ER compared to those of wt ER and purified ER.

The truncated YFP−SRC-3 construct was a kind gift from V. Giguère (McGill University, Montreal, PQ) and is here called YFP−RID. It consists of a YFP fused to the

N-terminus of the receptor interaction domain (RID) of SRC-3 (*16*).

Ligands. The ligands used in this study are 17β-estradiol (E2; Sigma), ICI 182,780 (ICI; Tocris) with the chemical name 7-α-[9-(4,4,5,5,5-pentafluoropentylsulfinyl)nonyl]estra-1,3,5(10)-triene-3,17-β-diol, and 4-hydroxytamoxifen (4OHT; Sigma).

FCS Experiments. For the concept of FCS, we refer to refs *17* and *18*. Briefly, a diluted sample of fluorophores, in our case YFP−ER inside nuclei of live cells, is excited in a diffraction-limited illumination volume of a focused laser beam (Figure 2d). In a typical FCS experiment, fluorescence intensity fluctuations are recorded with high time resolution and sensitivity, and analyzed in terms of their autocorrelation function (ACF). These intensity fluctuations arise from concentration fluctuations of particles diffusing into and out of the focal volume, and from photophysical processes changing the emission intensity of the particles. Thus, the correlation times obtained from appropriate models give access to the diffusion time or diffusion coefficient of the observed species. Because of its high sensitivity in the nanomolar range, FCS can yield information about biomolecular interactions at natural expression levels without the need of separating the different existing complexes.

FCS was performed on an LSM510 confocal laser scanning microscope equipped with a Confocor2 FCS-unit and a C-Apochromat 40× NA 1.2 water immersion objective (Zeiss). YFP was excited at 488 nm with an argon ion laser (≈3 kW/cm^2), and its fluorescence was detected through a pinhole (70 μm diameter) and a 530−600 nm band-pass filter. The excitation intensity was adjusted to maximize the detected counts per particle and at the same time to minimize both the occupation of triplet states and the rate of photobleaching. The LSM was used to localize cells with a sufficiently low expression level and to position the laser beam within the nucleus where FCS measurements were performed at room temperature (arrow in Figure 2b, c).

One requirement of FCS, i.e., to have a sample volume much larger than the observation volume, can be violated in intracellular measurements, especially in small compartments. The nuclei of MCF-7 cells chosen in this study were ∼5−10 times larger than the lateral and 2 times larger than the axial focus dimension. While the axial focus extension is on the same order of magnitude as the size of the nuclei, the ACF is mainly dominated by the lateral confinement of the focal volume. Thus, we expected the effect of the confined sample volume of the nucleus, other than limiting the number of available fluorophores, to be negligible. In fact, when the sample volume is reduced toward the observation volume, the ACF is expected to deviate from 0, its limiting value for long times. In the extreme case where the observation volume is smaller than the confocal volume, the particles cannot leave it any longer and the ACF is not suitable for deriving their diffusion dynamics. In our experiments, however, all ACFs completely dropped toward 0. This observation serves as an internal control that the observation volume was large enough to use the familiar formula for the FCS analysis.

For each series of FCS measurements, a standard calibration was performed using Rhodamine 6G in PBS solution at pH 7.4 (*19*). In this article, the molecular mobility is exclusively expressed in terms of the diffusion time τ_D. The corresponding diffusion coefficient D can be calculated with the relation $D = (21\ \mu s \times 280\ \mu m^2/s)/\tau_D$, which contains the diffusion time and diffusion coefficient of Rhodamine 6G of 21 μs and 280 μm^2/s, respectively.

In a typical experiment, 18 individual intensity time series were recorded over intervals of 5 s at each sample spot in one nucleus at a time resolution of 0.2 μs. Focal positions were chosen such that large speckles and nucleosomes were excluded from the focused laser beam. Direct focusing on speckles yielded substantial continuous bleaching, indicating that the speckles contain largely immobile components; photobleaching would lead to artifacts in the FCS analysis. In a series of FCS measurements, the very first data set taken at a particular position in the nucleus always contained an initial time interval dominated by photobleaching, and was therefore not included in the ACF analysis. To evaluate spatial variations of the observed diffusion time inside the nucleus, three measurements were performed at each of four different locations. Under the conditions described here, the variations between locations were on the same order of magnitude as the variations within locations (data not shown). Autocorrelation functions (ACFs) were computed from recordings of the fluctuating fluorescence intensity using commercial Zeiss software. The ACFs were then transferred to the data processing software Igor Pro (Wavemetrics) for further analysis.

Diffusion-Time Distribution Analysis. Details about model functions for the intensity ACF of an FCS experiment can be found in ref *20*. Typically, one or several photophysical dark states are taken into account, such as the triplet state or a state with a different degree of protonation, and one or several diffusing species with different diffusion constants. We found two parameters to be necessary and sufficient to describe the photophysics of YFP, in accordance with ref *21*. When we assumed one diffusing species to describe the data, which is equivalent to a population and time-averaged model, we obtained a broad and inhomogeneous distribution of diffusion times determined for each 5 s interval, indicating the presence of several species. Up to two diffusing species could be included in the fit to the superposition of all available ACFs per condition; more than two species resulted in overly large errors and no decrease in the reduced χ^2. The fast diffusive component of YFP−ER without any ligand (0.8 ± 0.1 ms) is compatible with the masses of YFP−ER monomers, dimers, and/or complexes with small chaperones, which are all indistinguishable in our FCS experiments (*22*). This diffusion time was kept fixed in the analysis, leaving the second diffusion time and its fraction as the only free fit parameters. The separation of receptors into a fast, slow, and immobile fraction is included in Supporting Information Figure 2. With the two-species model (one kept fixed), we could much better resolve the discrete diffusive states that were already visible in the distribution of a one-species model but with a smaller reduced χ^2. Our results clearly indicate the presence of more than two diffusive species, although even an averaged ACF did not allow for fitting a more complex model with sufficient reliability. We propose therefore for FCS of highly heterogeneous samples, such as a nucleus of a living cell, to analyze a distribution of diffusion times of very short time intervals [diffusion-time distribution analysis (DDA)], as opposed to the determination of a set of mean diffusion times from a multispecies model, averaged

over a long time and the whole ensemble. The latter includes maximum-entropy fitting of a multicomponent model to a single ACF (*23*), which we also applied to our data finding the same general trend as presented here but with much less pronounced results (data not shown). The time intervals in DDA should be kept as short as possible to obtain a very small subset of the whole distribution of diffusion times present in the sample, but long enough to collect a sufficiently long photon stream for a reliable determination of the diffusion time (in our case, 5 s). Short time intervals also reduce the effect of bleaching in each individual ACF, which is especially advantageous for intracellular measurements using YFP, where the level of bleaching is commonly rather high.

To construct diffusion-time distributions, we wanted to avoid the ambiguity commonly associated with the building of histograms, i.e., the choice of bin size and bin position, by averaging over several realizations of a histogram. By this and by choosing the bin size b according to $b = 1.06 \min(\sigma, R/1.34)n^{-1/5}$, we derived the optimal nonparametric estimator for the probability density function from our data (*24*). Here, σ is the standard deviation, R the interquartile range, and n the number of points entering the histogram. At this point, we stress that the smoothness of the histogram presented in this work is a result of the averaging process and not directly of the number of data points (see Figure 2g).

RESULTS AND DISCUSSION

To examine the complexity of ER mobility and interactions in nuclei of living cells, we applied FCS to monitor the diffusion of the YFP−ER fusion proteins (Figure 2a) and YFP−RID, the receptor interaction domain of SRC-3, transiently expressed in MCF-7 cells. FCS has already proven to be an invaluable quantitative tool for determining equilibrium and kinetic properties of molecular interactions in vitro (*25*, *26*) and in vivo (*27*−*29*). As shown previously, confocal microscopy revealed complete nuclear localization of YFP−ER, homogeneously distributed and excluded from nucleoli in the absence of ligand (Figure 2b); upon addition of the agonist E2, the well-documented speckled pattern appeared (Figure 2c) (*30*, *31*).

Fluorescence imaging was used to select cells with a sufficiently low expression level as required for FCS, i.e., approximately 100−1000 receptors per nucleus. The receptor concentration was determined on the basis of the number of molecules in the confocal volume. For the experiment, the focus was positioned inside the chosen nucleus some distance away from the speckles (arrow in panels b and c of Figure 2), and the fluctuating fluorescence intensity was recorded with sub-microsecond time resolution. The speckles were avoided because they contain a high concentration of immobilized receptors and because their origin is unclear.

Diffusion-Time Distribution Analysis. From the recorded intensity, time series autocorrelation functions (ACFs) were calculated (Figure 2e) and a two-species model was fitted to all our data to obtain a consistent set of data, even though the ACF of YFP−ER without any ligand is described well by a one-species model with a diffusion-time distribution that peaked at 2 ms having a shot-noise limited width. This τ_D corresponds to a complex size of ∼2 MDa, which is on the upper limit of the range that could be expected from previously found progesterone receptor complexes (*32*). We derived 18 ACFs per cell and between 150 and 250 ACFs for each ligand concentration. From each fit, we obtained the diffusion time and the fraction of the slow-moving component, while the diffusion time of the fast component was kept fixed to the median of the distribution without ligand (see Experimental Procedures). Subsequently determined diffusion times from six individual cells (Figure 2f) without ligand (black empty circles) and in the presence of 100 nM E2 (green filled circles) show no sign of correlation, trend, or cell-to-cell variation. The same data are summarized in histograms in Figure 2g, which are normalized to the total fraction of the slow component. Addition of E2 shifts the diffusion time to higher values, broadens the distribution, and creates additional peaks. The analysis of such a complex, multicomponent distribution obviously delivers more information than that conventionally obtained by computing very precisely the mean value of the distribution (black line at ∼7 ms in Figure 2g).

Ligand-Dependent ER Interactions. A reduction in ER mobility upon addition of different ligands has been observed previously by live-cell fluorescence microscopy in conjunction with qualitative fluorescence recovery after photobleaching (FRAP). These studies have revealed the dynamic nature of steroid receptor (SR) interactions with cofactors and chromatin and its relatively high intranuclear mobility (*31*, *33*, *34*). Further indications of ligand-induced molecular interactions came from fluorescence resonance energy transfer (FRET) experiments (*35*, *36*). However, both types of assays did not provide detailed quantitative information about SR interactions and mobility, and delivered only an overall and simplified picture of SR interactions with cofactor proteins.

The ligands used in this study include the full agonist 17β-estradiol (E2), the antagonist ICI 182,780 (ICI), approved by the U.S. Food and Drug Administration (FDA) as a treatment for breast cancer under the generic name Fulvestrant (AstraZeneca), and the partial antagonist 4-hydroxytamoxifen (4OHT), currently one of the most frequently prescribed drugs against breast cancer.

Even in the absence of ligand, the mobility distribution of YFP−ER is not completely homogeneous, as compared, for example, to only YFP in the nucleus (data not shown), and consists of a major peak at ∼2.5 ms, and a small shoulder at ∼5 ms (dashed black line in Figure 3a). This finding provides evidence that ER is present in the nucleus not in one single state but rather in at least two different states as a result of either hindered diffusion or additional interactions. Increasing the concentration of the agonist E2 results in a gradual shift toward longer diffusion times and in the appearance of multiple side peaks, which occur consistently at the same position for different ligand concentrations (green area and green line in Figure 3a). Addition of E2 to intracellular YFP did not change its mobility (data not shown). We attribute these peaks to discrete complexes of YFP−ER with cofactor proteins and/or chaperones with well-defined sizes, as well as to specific but transient interactions with chromatin and nuclear structures with well-defined residence times. Unspecific interactions and a broad range of complexes would give rise to an unstructured diffusion-time distribution. The partial antagonist and selective estrogen

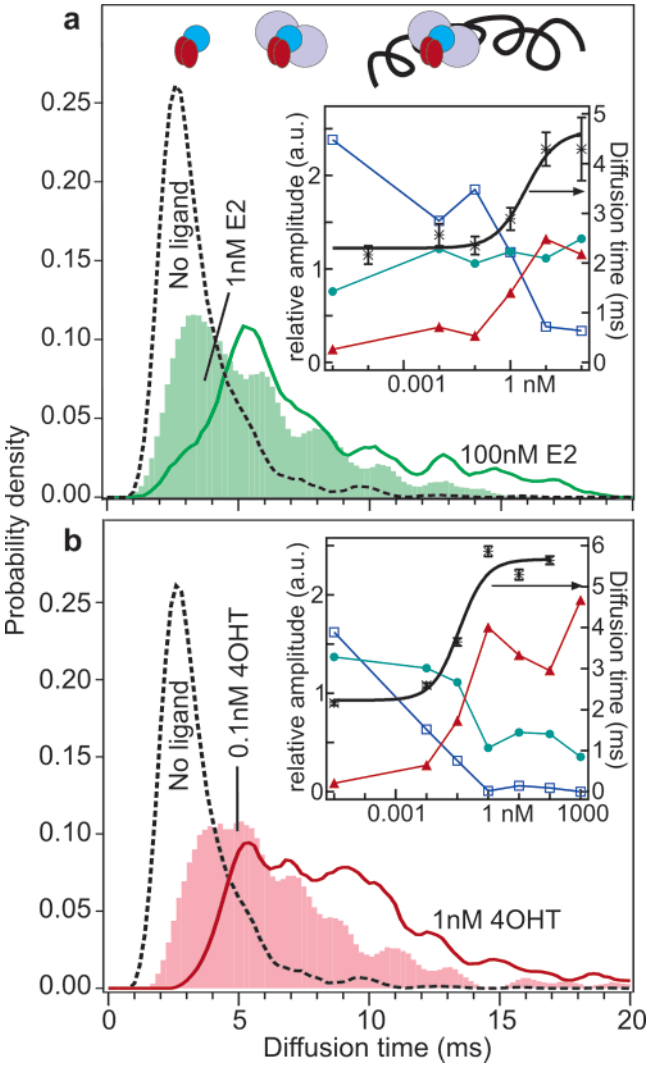

FIGURE 3: Diffusion-time distributions of YFP−ER and effect of increasing ligand concentrations. (a) Three distributions at different concentrations of the agonist E2: 0 (dashed line), 1 (filled bars), and 100 nM (solid line). Discrete peaks appear at the same position for the two concentrations but with different amplitudes. At the top are cartoons describing the possible origin of the reduced mobility (from left to right): small complexes become larger complexes, and eventually bind more often and longer transiently to chromatin. (b) Three distributions at different concentrations of 4OHT: 0 (dashed line), 0.1 (filled bars), and 1 nM (solid line). Again, discrete peaks appear at the same position for the two concentrations but with different amplitudes. In both cases, a broadening of the distribution with an increase in ligand concentration and a shift toward larger diffusion times is observed. The mobility pattern of YFP−ER in the presence of agonist E2 is different from the pattern in the presence of partial antagonist 4OHT; i.e., the peaks are characteristic of the ligand. The insets show concentration response curves of ER mobility in the presence of E2 (a) and 4OHT (b). Median of the diffusion time (black, right axis), as well as the cumulative amplitude in three diffusion-time intervals (left axis): (a) 0−4 (blue), 4−7 (green), and 7−15 ms (red) and (b) 0−3 (blue), 3−5 (green), and 8−15 ms (red).

receptor modulator 4OHT also induces the formation of discrete complexes (Figure 3b), but with a diffusion pattern different from that of E2. A small amplitude of the original peak at ~2.5 ms is still present even at 100 nM E2, whereas in the presence of only 1 nM 4OHT, this peak vanished completely. By comparing the different distributions at different concentrations of various ligands, we can distinguish and investigate their effect on the mobility of YFP−ER. The different diffusion times of the mobility states in the presence of E2 and 4OHT are likely due to the formation of different mobile complexes between ER and co-activators (E2) or co-repressors (4OHT), similar to the recruitment of co-repressors to 4OHT-bound ER (*37*, *38*) and the recruitment of co-activators to E2-bound ER (*2*, *39*). Another aspect of the two ligands that could affect their complex formation is that E2 downregulates ER while 4OHT stabilizes ER levels in the nucleus (*40*). In fact, we find the presence of a large fraction of ER with a diffusion time from 8 to 12 ms characteristic of antagonists (4OHT and ICI), while agonists (E2, coumestrol) do not induce the formation of ER interactions in this region but rather create a major fraction around 4−7 ms (a detailed account of the ligand dependence of ER diffusion-time distributions will be published elsewhere).

Although we cannot tell at this stage how many different protein complexes are represented by each peak and which proteins constitute the complexes (see below), we can reasonably speculate about the nature of the observed mobility states since we know the masses of several of the potential ER interaction partners, as well as the diffusion coefficient of chromatin (*41*). There are further indications that the apparent viscosity that a macromolecule experiences inside the nucleus does not depend on its size, in contrast to the situation in the cytoplasm (*42*, *43*). With FCS, one determines in general the mobility of labeled particles expressed in terms of the diffusion time which, for freely diffusing particles, depends on the size of the particle, the viscosity of the medium, and the temperature. When the particle is binding to and dissociating from other components, mobile or immobile, the apparent diffusion time will be influenced according to the residence time and the second component's mobility. Assuming the increase in diffusion time is solely caused by an increase in the size of the complexes in which ER is present, a diffusion time of 10 ms would correspond to a mass of ~270 MDa, which seems to be unreasonably high for native protein complexes. Transient association with chromatin on the other hand could be responsible for a substantially reduced average mobility. The interaction should be transient, as only mobile molecules contribute to the FCS signal, while permanently chromatin-associated receptors are bleached. To interpret our experimental finding, we consider an ensemble of three classes of particles: unperturbed YFP−ER complexes consisting of YFP−ER dimers and chaperones (τ_D = 2.5 ms), ligand-induced complexes containing YFP−ER with a mass of 10 MDa (τ_D = 3.3 ms), and chromatin-bound YFP−ER with a diffusion coefficient of 5×10^{-4} $\mu m^2/s$. With these assumptions, a measured diffusion time of 10 ms would require the receptor to be bound on chromatin between 60 and 80% of the time, and to be in ligand-induced mobile complexes for less than 40% of the time.

A key difference of our approach to previous FRAP experiments is that we are able to detect and distinguish particular states of mobility via DDA. A multicomponent mixture of diffusing particles is not easily resolved with FRAP (*44*), and has to our knowledge not been accomplished yet in a living cell. Also, recovery times from FRAP experiments usually depend on the actual instrumental parameters, whereas the diffusion times or diffusion coefficients obtained here can be readily compared with results

from other laboratories. Moreover, only relatively slow processes (>0.1 s) in relatively strongly expressing cells are accessible with FRAP, with a relatively low spatial resolution, while FCS allows for the investigation of processes down to a 10 μs time scale in weakly expressing cells with a spatial resolution of a few hundred nanometers.

The ligand-dependent equilibrium distributions of diffusion times in Figure 3 represent the first new quantitative finding on the nature of ER interactions in the nucleus. From the concentration dependence of the distributions, dose or concentration response curves (CRCs) can be obtained in vivo for each ligand (Figure 3 insets) in several ways: the CRC of the median (black stars and line, right axis), the CRC of the cumulative amplitude in different diffusion-time intervals (left axis; see the figure legend), or the CRC of individual peaks. In the case of E2, the half-maximal effective concentration (EC_{50}) of the median is similar to the EC_{50} of individual intervals (approximately 1 nM), and consistent with previous findings (*45*). The situation is slightly different when 4OHT is added. While the median and the slow-moving fraction above 5 ms react in a manner similar to that of the partial antagonist (*45*), the magnitude of the initial peak at 2.5 ms decreases already at concentrations below 10 pM (Figure 3b inset, blue squares), which might be an indication of a previously undiscovered high-affinity mode of action of 4OHT on ER.

ER Cofactor Interactions. To identify some of the observed complexes and determine their composition, we investigated the diffusion-time distribution of a fluorescent version of the receptor interaction domain of the ER−cofactor SRC-3 (YFP−RID). Overlapping regions of the distribution of ER and RID indicate that they exist in complexes with similar mobility and that they might be contained in the same complex. Therefore, comparative DDA of labeled ER cofactors allows for the identification of those molecular complexes which contain both ER and the respective cofactor and those which contain either only ER or only the cofactor. The action of E2 and ICI on the mobility of YFP−RID in the presence of endogenous ER is of particular interest for testing our approach, since ICI is an antagonist known to disrupt the ER−SRC interaction (*16*) while E2 induces this interaction.

In the absence of ligand, the majority of YFP−RID exhibits a diffusion time slightly shorter than that of YFP−ER (1.5 ms compared to 2.5 ms), which is a definite sign that they are not interacting permanently with each other (Figure 4a). This major peak is probably due to isolated YFP−RID. A minor fraction of ~15% already seems to interact with YFP−ER, represented by the shoulder at 3.5 ms. DDA results for additionally coexpressed nonlabeled ER support this hypothesis (see Supporting Information Figure 1). Upon addition of 100 nM E2, the lower half of the major peak of YFP−RID at 1 ms decreases to a probability density of 0.06 and the remaining fraction at 2 ms to below 0.02. In addition, the distribution increases in the same regions where a significant fraction of YFP−ER complexes are found (between 4 and 8 ms and at 10 ms). The higher amplitude for YFP−ER in this interval reflects a larger number of complexes due to the different expression levels of ER and RID in the two experiments. Our interpretation is that E2 induces YFP−ER and YFP−RID to associate in common complexes with a mobility in the range of 4−11 ms.

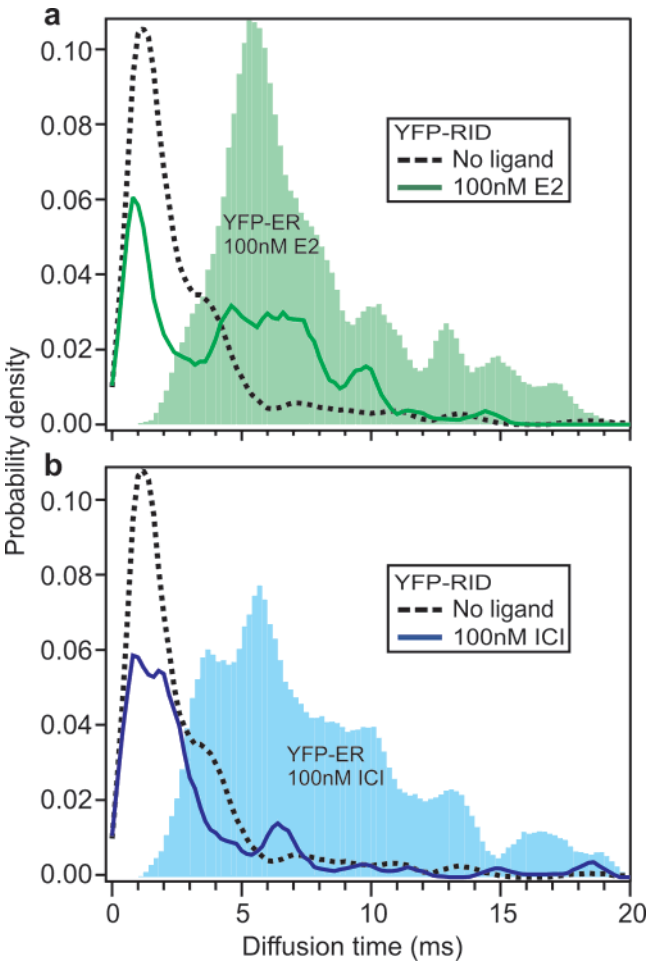

FIGURE 4: Diffusion-time distribution of the receptor interaction domain (YFP−RID) of cofactor SRC-3 in the absence (dotted line) and presence (solid line) of agonist E2 (a) and antagonist ICI (b). The distribution of YFP−ER under the same conditions is shown for comparison (filled bars). Addition of E2 creates YFP−RID complexes with a diffusion time in the range from 5 to 8 ms, the same range of mobility that is found predominantly for YFP−ER. In contrast, addition of ICI does not create these complexes but rather decreases the amount of YFP−RID with a diffusion time of ~4 ms.

However, YFP−RID is also present in an unbound form, like in the absence of E2 (1 ms), and YFP−ER also exists in slower diffusion states (>10 ms), possibly in complex with proteasomes and bound to chromatin or other nuclear structures (*31*, *46*, *47*).

A different picture arises when 100 nM ICI is added to the cells (Figure 4b). Both parts of the major peak decrease in magnitude (1−2 ms) and the shoulder at 3.5 ms vanishes. The fast fraction increases, and no new complexes are formed between 4 and 11 ms. This can be explained by the fact that ICI destabilizes complexes of RID with ER. Taken together, whereas ICI removes common protein complexes in the diffusion-time distribution of ER and RID, E2 creates novel complexes as compared to the situation without ligand.

CONCLUSION

We have discovered the simultaneous existence of multiple discrete interactions of ER with nuclear components in living breast cancer cells. The population of these states varies with increasing ligand concentrations, and different ligands induce the formation of distinct and characteristic complexes. The

fastest components most likely comprise ER dimers and chaperones; intermediate components are probably complexes of ER with several cofactors, and there are strong indications that the slowest components are caused by the transient interaction of ER−cofactor complexes with chromatin or other nuclear structures. We were able to retrieve these findings with the help of a new approach to FCS analysis of highly heterogeneous samples, diffusion-time distribution analysis (DDA). The information content presented by DDA is superior to the conventional evaluation of FCS data and to FRAP, where only average values are determined and no information about higher moments of distributions is obtained. Thus, transfer of the concept of DDA to other local and fast fluorescence techniques, such as fluorescence cross-correlation spectroscopy (*29*) or photon counting statistics methods (*48*, *49*), can advance these techniques. By using a fluorescent cofactor and comparative DDA, we have built the foundation for elucidating step-by-step simultaneously existing ER−cofactor complexes, their evolution with time, and their dependence, for instance, on growth factors and acetylation or phosphorylation of the constituents. Moreover, DDA following silencing of the genes of individual or multiple, known or putative ER interaction partners with RNAi technology bears an enormous opportunity to complement and extend this approach. However, to obtain an extended picture of ER mobility, it will be challenging to determine the diffusion coefficient and binding events of individual molecules as a function of time. Once this is possible, in the future the single-molecule mobility distribution will most likely be even broader and more structured than the one obtained here. With the derivation of CRCs for several ligands and separately for particular subsets of the multicomponent distribution of diffusion times, we have demonstrated the power of our method to determine thermodynamic quantities, i.e., effective dissociation constants, of ligand-induced interactions of a protein, simultaneously with several other proteins and chromatin, noninvasively in living cells under natural expression levels. With a variation of the recording time of the individual fluorescence data, DDA promises to access kinetic parameters, like dissociation rate constants between two proteins, and thus to become a powerful tool for disentangling complex biochemical networks and to be used in modern high-content screening applications.

ACKNOWLEDGMENT

We thank Vincent Giguère for the kind gift of the YFP−RID plasmid, Beatrice Desvèrgne, Laurent Gelman, and Jerome Feige for stimulating discussions, and Thorsten Wohland for advice concerning FCS. We thank further the colleagues in our group for helpful discussions, especially Daniel Abankwa, Ruud Hovius, Jean-Manuel Segura, and Wolf-Peter Ulrich.

SUPPORTING INFORMATION AVAILABLE

Additional figures presenting diffusion-time distributions and the partitioning of ER into immobile, fast, and slow fractions. This material is available free of charge via the Internet at http://pubs.acs.org.

REFERENCES

1. McKenna, N. J., and O'Malley, B. W. (2002) Combinatorial control of gene expression by nuclear receptors and coregulators, *Cell 108*, 465−474.
2. Metivier, R., Penot, G., Hubner, M. R., Reid, G., Brand, H., Kos, M., and Gannon, F. (2003) Estrogen receptor-α directs ordered, cyclical, and combinatorial recruitment of cofactors on a natural target promoter, *Cell 115*, 751−763.
3. Hager, G. L., Nagaich, A. K., Johnson, T. A., Walker, D. A., and John, S. (2004) Dynamics of nuclear receptor movement and transcription, *Biochim. Biophys. Acta 1677*, 46−51.
4. Tsai, M. J., and O'Malley, B. W. (1994) Molecular mechanisms of action of steroid/thyroid receptor superfamily members, *Annu. Rev. Biochem. 63*, 451−486.
5. Gronemeyer, H., Gustafsson, J. A., and Laudet, V. (2004) Principles for modulation of the nuclear receptor superfamily, *Nat. Rev. Drug Discovery 3*, 950−964.
6. Damstra, T. (2002) *Global Assessment of the State-of-the-Science of Endocrine Disruptors*, World Health Organization, http://www.who.int/ipcs/publications/new_issues/endocrine_disruptors/en/.
7. Markey, C. M., Rubin, B. S., Soto, A. M., and Sonnenschein, C. (2002) Endocrine disruptors: From Wingspread to environmental developmental biology, *J. Steroid Biochem. Mol. Biol. 83*, 235−244.
8. Zhu, H., Bilgin, M., and Snyder, M. (2003) Proteomics, *Annu. Rev. Biochem. 72*, 783−812.
9. Gavin, A. C., Bosche, M., Krause, R., Grandi, P., Marzioch, M., Bauer, A., Schultz, J., Rick, J. M., Michon, A. M., Cruciat, C. M., Remor, M., Hofert, C., Schelder, M., Brajenovic, M., Ruffner, H., Merino, A., Klein, K., Hudak, M., Dickson, D., Rudi, T., Gnau, V., Bauch, A., Bastuck, S., Huhse, B., Leutwein, C., Heurtier, M. A., Copley, R. R., Edelmann, A., Querfurth, E., Rybin, V., Drewes, G., Raida, M., Bouwmeester, T., Bork, P., Seraphin, B., Kuster, B., Neubauer, G., and Superti-Furga, G. (2002) Functional organization of the yeast proteome by systematic analysis of protein complexes, *Nature 415*, 141−147.
10. Aebersold, R., and Mann, M. (2003) Mass spectrometry-based proteomics, *Nature 422*, 198−207.
11. Lidke, D. S., Nagy, P., Heintzmann, R., Arndt-Jovin, D. J., Post, J. N., Grecco, H. E., Jares-Erijman, E. A., and Jovin, T. M. (2004) Quantum dot ligands provide new insights into erbB/HER receptor-mediated signal transduction, *Nat. Biotechnol. 22*, 198−203.
12. Guignet, E. G., Hovius, R., and Vogel, H. (2004) Reversible site-selective labeling of membrane proteins in live cells, *Nat. Biotechnol. 22*, 440−444.
13. Nilsson, S., Makela, S., Treuter, E., Tujague, M., Thomsen, J., Andersson, G., Enmark, E., Pettersson, K., Warner, M., and Gustafsson, J. A. (2001) Mechanisms of estrogen action, *Physiol. Rev. 81*, 1535−1565.
14. Michnick, S. W. (2004) Proteomics in living cells, *Drug Discovery Today 9*, 262−267.
15. Schreiber, E., Matthias, P., Muller, M. M., and Schaffner, W. (1989) Rapid detection of octamer binding proteins with 'mini-extracts', prepared from a small number of cells, *Nucleic Acids Res. 17*, 6419.
16. Bai, Y., and Giguere, V. (2003) Isoform-Selective Interactions between Estrogen Receptors and Steroid Receptor Coactivators Promoted by Estradiol and ErbB-2 Signaling in Living Cells, *Mol. Endocrinol. 17*, 589−599.
17. Rigler, R., and Elson, E. S. (2001) *Fluorescence Correlation Spectroscopy: Theory and Applications*, 1st ed., Vol. 65, Springer-Verlag, Berlin.
18. Krichevsky, O., and Bonnet, G. (2002) Fluorescence correlation spectroscopy: The technique and its applications, *Rep. Prog. Phys. 65*, 251−297.
19. Rigler, R., Mets, U., Widengren, J., and Kask, P. (1993) Fluorescence Correlation Spectroscopy with High Count Rate and Low-Background: Analysis of Translational Diffusion, *Eur. Biophys. J. 22*, 169−175.
20. Wachsmuth, M., Waldeck, W., and Langowski, J. (2000) Anomalous diffusion of fluorescent probes inside living cell nuclei investigated by spatially-resolved fluorescence correlation spectroscopy, *J. Mol. Biol. 298*, 677−689.
21. Schwille, P., Kummer, S., Heikal, A. A., Moerner, W. E., and Webb, W. W. (2000) Fluorescence correlation spectroscopy reveals fast optical excitation-driven intramolecular dynamics of yellow fluorescent proteins, *Proc. Natl. Acad. Sci. U.S.A. 97*, 151−156.
22. Meseth, U., Wohland, T., Rigler, R., and Vogel, H. (1999) Resolution of fluorescence correlation measurements, *Biophys. J. 76*, 1619−1631.

23. Sengupta, P., Garai, K., Balaji, J., Periasamy, N., and Maiti, S. (2003) Measuring size distribution in highly heterogeneous systems with fluorescence correlation spectroscopy, *Biophys. J. 84*, 1977−1984.
24. Venables, W. N., and Ripley, B. D. (1997) *Modern applied statistics with S-PLUS*, 2nd ed., Springer-Verlag, New York.
25. Rauer, B., Neumann, E., Widengren, J., and Rigler, R. (1996) Fluorescence correlation spectrometry of the interaction kinetics of tetramethylrhodamin α-bungarotoxin with *Torpedo californica* acetylcholine receptor, *Biophys. Chem. 58*, 3−12.
26. Wohland, T., Friedrich, K., Hovius, R., and Vogel, H. (1999) Study of ligand−receptor interactions by fluorescence correlation spectroscopy with different fluorophores: Evidence that the homopentameric 5-hydroxytryptamine type 3As receptor binds only one ligand, *Biochemistry 38*, 8671−8681.
27. Berland, K. M., So, P. T., and Gratton, E. (1995) Two-photon fluorescence correlation spectroscopy: Method and application to the intracellular environment, *Biophys. J. 68*, 694−701.
28. Weiss, M., Hashimoto, H., and Nilsson, T. (2003) Anomalous protein diffusion in living cells as seen by fluorescence correlation spectroscopy, *Biophys. J. 84*, 4043−4052.
29. Bacia, K., Scherfeld, D., Kahya, N., and Schwille, P. (2004) Fluorescence correlation spectroscopy relates rafts in model and native membranes, *Biophys. J. 87*, 1034−1043.
30. Htun, H., Holth, L. T., Walker, D., Davie, J. R., and Hager, G. L. (1999) Direct visualization of the human estrogen receptor α reveals a role for ligand in the nuclear distribution of the receptor, *Mol. Biol. Cell 10*, 471−486.
31. Stenoien, D. L., Patel, K., Mancini, M. G., Dutertre, M., Smith, C. L., O'Malley, B. W., and Mancini, M. A. (2001) FRAP reveals that mobility of oestrogen receptor-α is ligand- and proteasome-dependent, *Nat. Cell Biol. 3*, 15−23.
32. McKenna, N. J., Nawaz, Z., Tsai, S. Y., Tsai, M. J., and O'Malley, B. W. (1998) Distinct steady-state nuclear receptor coregulator complexes exist *in vivo*, *Proc. Natl. Acad. Sci. U.S.A. 95*, 11697−11702.
33. McNally, J. G., Muller, W. G., Walker, D., Wolford, R., and Hager, G. L. (2000) The glucocorticoid receptor: Rapid exchange with regulatory sites in living cells, *Science 287*, 1262−1265.
34. Elbi, C., Walker, D. A., Romero, G., Sullivan, W. P., Toft, D. O., Hager, G. L., and DeFranco, D. B. (2004) Molecular chaperones function as steroid receptor nuclear mobility factors, *Proc. Natl. Acad. Sci. U.S.A. 101*, 2876−2881.
35. Llopis, J., Westin, S., Ricote, M., Wang, Z., Cho, C. Y., Kurokawa, R., Mullen, T. M., Rose, D. W., Rosenfeld, M. G., Tsien, R. Y., Glass, C. K., and Wang, J. (2000) Ligand-dependent interactions of coactivators steroid receptor coactivator-1 and peroxisome proliferator-activated receptor binding protein with nuclear hormone receptors can be imaged in live cells and are required for transcription, *Proc. Natl. Acad. Sci. U.S.A. 97*, 4363−4368.
36. Weatherman, R. V., Chang, C. Y., Clegg, N. J., Carroll, D. C., Day, R. N., Baxter, J. D., McDonnell, D. P., Scanlan, T. S., and Schaufele, F. (2002) Ligand-selective interactions of ER detected in living cells by fluorescence resonance energy transfer, *Mol. Endocrinol. 16*, 487−496.
37. Webb, P., Nguyen, P., and Kushner, P. J. (2003) Differential SERM effects on corepressor binding dictate ER α activity *in vivo*, *J. Biol. Chem. 278*, 6912−6920.
38. Liu, X. F., and Bagchi, M. K. (2004) Recruitment of distinct chromatin-modifying complexes by tamoxifen-complexed estrogen receptor at natural target gene promoters in vivo, *J. Biol. Chem. 279*, 15050−15058.
39. Shang, Y., Hu, X., DiRenzo, J., Lazar, M. A., and Brown, M. (2000) Cofactor dynamics and sufficiency in estrogen receptor-regulated transcription, *Cell 103*, 843−852.
40. Muller, V., Jensen, E. V., and Knabbe, C. (1998) Partial antagonism between steroidal and nonsteroidal antiestrogens in human breast cancer cell lines, *Cancer Res. 58*, 263−267.
41. Davis, S. K., and Bardeen, C. J. (2004) The connection between chromatin motion on the 100 nm length scale and core histone dynamics in live XTC-2 cells and isolated nuclei, *Biophys. J. 86*, 555−564.
42. Seksek, O., Biwersi, J., and Verkman, A. S. (1997) Translational diffusion of macromolecule-sized solutes in cytoplasm and nucleus, *J. Cell Biol. 138*, 131−142.
43. Verkman, A. S. (2002) Solute and macromolecule diffusion in cellular aqueous compartments, *Trends Biochem. Sci. 27*, 27−33.
44. Starr, T. E., and Thompson, N. L. (2002) Fluorescence pattern photobleaching recovery for samples with multi-component diffusion, *Biophys. Chem. 97*, 29−44.
45. Sun, J., Meyers, M. J., Fink, B. E., Rajendran, R., Katzenellenbogen, J. A., and Katzenellenbogen, B. S. (1999) Novel ligands that function as selective estrogens or antiestrogens for estrogen receptor-α or estrogen receptor-β, *Endocrinology 140*, 800−804.
46. Lonard, D. M., Nawaz, Z., Smith, C. L., and O'Malley, B. W. (2000) The 26S proteasome is required for estrogen receptor-α and coactivator turnover and for efficient estrogen receptor-α transactivation, *Mol. Cell 5*, 939−948.
47. Reid, G., Hubner, M. R., Metivier, R., Brand, H., Denger, S., Manu, D., Beaudouin, J., Ellenberg, J., and Gannon, F. (2003) Cyclic, proteasome-mediated turnover of unliganded and liganded ERα on responsive promoters is an integral feature of estrogen signaling, *Mol. Cell 11*, 695−707.
48. Chen, Y., Muller, J. D., Berland, K. M., and Gratton, E. (1999) Fluorescence fluctuation spectroscopy, *Methods 19*, 234−252.
49. Palo, K., Mets, U., Jager, S., Kask, P., and Gall, K. (2000) Fluorescence intensity multiple distributions analysis: Concurrent determination of diffusion times and molecular brightness, *Biophys. J. 79*, 2858−2866.
50. Kraichely, D. M., Sun, J., Katzenellenbogen, J. A., and Katzenellenbogen, B. S. (2000) Conformational changes and coactivator recruitment by novel ligands for estrogen receptor-α and estrogen receptor-β: Correlations with biological character and distinct differences among SRC coactivator family members, *Endocrinology 141*, 3534−3545.
51. Onate, S. A., Tsai, S. Y., Tsai, M. J., and O'Malley, B. W. (1995) Sequence and characterization of a coactivator for the steroid hormone receptor superfamily, *Science 270*, 1354−1357.

BI050744V